Supporting Information

Keimpema et al. 10.1073/pnas.1212563110

SI Materials and Methods

Mice, Drug Treatment, and Ethical Approval of Experimental Studies. Tissues from C57Bl6/J, choline acetyltransferase (ChAT)(BAC)-EGFP (1), CB_1 cannabinoid receptor $(CB_1R)^{-/-}$ on CD1 (2) or C57Bl6/J (3) backgrounds, AD11 mice (2–3 mo of age), which postnatally express a recombinant anti–nerve growth factor (NGF) antibody (4, 5), and corresponding wild-type littermates were characterized and processed as described (6, 7).

AM 251 (3 mg/kg in 1:1 triethylene glycol:physiological saline) (8) was administered i.p. daily to wild-type dams (C57Bl6/J background; $n = 3$) during the period of embryonic day (E)5.5 to E17.5. Embryos were harvested on E18.5. We used male fetuses because these are particularly prone to developmental deficits attributable to the pharmacological manipulation of prenatal endocannabinoid signaling or exposure to Δ^9-tetrahydrocannabinol (9–11). The use of $CB_1R^{-/-}$ mice on C57Bl6/J (Fig. 1 *D–F*) and CD1 (Fig. 1 *G–I*) backgrounds in separate experiments is justified because these strains present comparable developmental (e.g., axon guidance) defects (12). The Home Office of the United Kingdom approved the experimental designs and procedures. All procedures adhered to the European Communities Council Directive (86/609/EEC). Efforts were made to minimize the number of animals and their suffering throughout the experiments.

Histo- and Cytochemistry. Multiple immunofluorescence labeling of fetal mouse brains, cultured basal forebrain neurons, and rat pheochromocytoma cell line 12 (PC12) cells was performed by applying select mixtures of affinity-purified antibodies (Table S1) (6, 7, 13). DyLight488/549/649- or carbocyanine (Cy)2/3/5-conjugated secondary antibodies (Jackson ImmunoResearch) were used to visualize primary antibody binding. F-actin was revealed by phalloidin-560 (1:500 for 1 h; Invitrogen). In situ hybridization was undertaken by using digoxigenin-labeled riboprobes against the mouse CB_1R (12, 14). After hybridization, sections were incubated with a sheep anti–digoxigenin-Fab antibody fragment conjugated to alkaline phosphatase (Roche). The staining was developed with 5-bromo-4-chloro-indoylphosphate and nitroblue tetrazolium as substrates (sense control: Fig. S1*A*$_1$). $CB_1R^{-/-}$ sections were used as negative controls in both immunofluorescence (Fig. S1 *G–H*$_1$′) and in situ hybridization histochemistry (15). Hoechst 33,342 (Sigma) was routinely used as nuclear counterstain.

Laser-Scanning Microscopy and Quantitative Morphometry. Images were acquired on a 710LSM confocal laser-scanning microscope (Zeiss). Emission spectra for each dye were limited as follows: Hoechst (420–480 nm), Cy2/DyLight488 (505–530 nm), Cy3/DyLight549 (560–610 nm), and Cy5/DyLight649 (650–720 nm) (13). Image surveys were generated using the tile scan function with optical zoom ranging from 0.6× to 1.5× at 10× primary magnification (objective: EC Plan-Neofluar 10×/0.30).

Colocalization of select histochemical marker pairs [e.g., CB_1R/EGFP, breast cancer type 1 susceptibility protein (BRCA1)/ChAT] was verified by capturing serial orthogonal z images (z stacks) at 63× primary magnification (pinhole: 20 μm; 2048 × 2048 pixel resolution), resulting in image stacks usually containing 5–30 z levels scaled as $x = 0.104$ μm, $y = 0.104$ μm, and $z = 0.324$ μm. The coexistence of immunosignals was accepted if these were present without physical signal separation in ≤1.0-μm optical slices at 40× (Plan-Neofluar 40×/1.30) or 63× (Plan-Apochromat 63×/1.40) primary magnification and overlapped in all three (x, y, and z) dimensions within individual cellular domains (Fig. 1 *B*$_1$*–C*$_2$). Images were processed using the ZEN2010 software package (Zeiss). At least $n = 3$ embryos per time point per genotype were processed.

The topographic location of $p75^{NTR+}$/$ChAT^+$ neurons in the fetal striatum (rostral to the commissure anterior, Fig. 1 *D–E*$_2$) was determined in serial coronal sections (140-μm intersection interval; $n = 2$–4 sections per fetal mouse brain) of $CB_1R^{-/-}$ and wild-type fetuses (E18.5) with or without maternal AM 251 exposure. The distribution of $p75^{NTR+}$/$ChAT^+$ neurons was mapped onto generic brain overview plates of the corresponding developmental stage (16). The density of striatal $p75^{NTR+}$ neurons was expressed as the percentage of $ChAT^+$ cells counted in the same section (note that all $p75^{NTR+}$ neurons expressed ChAT although at variable levels; Fig. S1*C*). Data were then presented as the percentage of $ChAT^+$ neuron density/striatum after averaging cell counts from both striata in each fetus (Fig. 1*E*). The density of $ChAT^+$ perikarya in the striatum of adult $CB_1R^{-/-}$ and wild-type CD1 mice ($n = 3$/group) was expressed after normalizing the sampling area to 1 mm^2. At least three sagittal sections per mouse were analyzed at select coordinates (17) spanning the striatum (Fig. 1 *G* and *G*$_1$ and Fig. S2 *D–D*$_2$).

The density of $ChAT^+$ innervation in the strata pyramidale and radiatum of the CA1 hippocampal subfield in adult wild-type and $CB_1R^{-/-}$ mice (2–3 mo of age) (18) were analyzed at 63× primary magnification (1 μm optical thickness; $n = 3$ sections per animal; $n = 3$ animals per genotype). Data were expressed as the number of $ChAT^+$ profiles per 1,000 μm^2 using ImageJ (Version 1.45s; Fig. 1 *H–H*$_2$ and Fig. S2*E*). MGL^+ puncta were captured in the CA1 stratum pyramidale of adult wild-type and $CB_1R^{-/-}$ mice (2–3 mo of age) at 63× primary magnification, and their density was determined offline using University of Texas Health Science Center at San Antonio (UTHSCSA) ImageTool (Version 3.00; http://compdent.uthscsa.edu/ITDownload.asp). Corresponding data were presented as the number of MGL^+ profiles per 1 μm^2 (Fig. 1*I* and Fig. S2 *F–G*$_1$).

Neurite morphology of $ChAT^+$ neurons in the medial septum (MS)/horizontal diagonal band of Broca (HDB) complex of E18.5 wild-type and $CB_1R^{-/-}$ fetuses was determined by Sholl analysis (19). A series of concentric rings (10 μm apart) was centered on cholinergic somata ($n = 30$–35 cells per animal; $n = 3$ fetuses per group) with emanating processes counted when crossing a concentric circle and subsequently plotted (representative cell morphology: Fig. 1*F*; quantitative data: Fig. 1*F*$_1$).

The intensity of CB_1R, *sn*-1-diacylglycerol lipase (DAGL)α, DAGLβ, and MGL immunoreactivities along the primary vesicular acetylcholine transporter $(VAChT)^+$ neurite ($n = 6$–8 per marker) of cholinergic neurons cultured for 4 d in vitro (DIV) was measured by obtaining a plot profile starting at the growth cone's filopodial tip and along the distal axon segment (6) (total length, 40 μm; Fig. 2*C*$_4$; ImageJ 1.45s). Data were presented as arbitrary units of unscaled immunofluorescence intensities (range: 0–90 gray scale units).

The density of MGL immunoreactivity in layer 5 of the somatosensory cortex of presymptomatic AD11 ($n = 5$) and wild-type mice ($n = 3$) was determined by capturing images at 63× primary magnification (1-μm optical thickness; $n = 3$–4 sections per animal; 2048 × 2048 pixel resolution) under uniform laser-excitation (Fig. 4 *E–F*$_2$). High-resolution graphic images were digitized, underwent uniform threshold adjustment to precisely discern MGL^+ structures, and exported into the UTHSCSA ImageTool (Version 3.00; http://compdent.uthscsa.edu/ITDownload.asp)

to determine the number of MGL^+ profiles per unitary surface area (2,315 μm^2) (see ref. 20 for procedural details). The number of MGL^+ puncta along $ChAT^+$ dendrites was counted and normalized to 100-μm-long dendrite segments (Fig. S5 *D–D$_1$*). The brightness or contrast of confocal laser-scanning micrographs was occasionally linearly enhanced. Multipanel figures were assembled in CorelDraw X5 (Corel).

Liquid Chromatography–Tandem Mass Spectrometry. In vitro concentrations of 2-arachidonoyl glycerol (2-AG) (Fig. 3*E*) were determined from cell pellets of basal forebrain cultures (10^6 cells per well in six-well plates; triplicate measurements from two independent experiments) using a solid-phase extraction liquid chromatography–tandem mass spectrometry method (6, 21). Levels of 2-AG from NGF-treated (4 DIV) primary neurons were normalized to nontreated controls (Fig. 3*E*).

Microarray Analysis. Basal forebrain, hippocampus, and neocortex were rapidly dissected after decapitation. Total RNA was isolated using TRIzol (Invitrogen) and DNase treated on Qiagen columns. RNA quality was checked using an Agilent BioAnalyzer 2100. Samples with an RNA integrity index of <8.0 were discarded. Aliquots from the same RNA sample, prepared (and pooled) from $n = 2$ whole brains of wild-type mice, were used in all hybridizations as reference. Gene expression profiling was performed using the two-color protocol by Agilent with reference experimental design (22). AD11 samples were labeled with Cy5 fluorochrome. AD11 transgenic controls, as well as reference samples, were labeled with Cy3. Cy3- and Cy5-labeled cRNAs were hybridized to Agilent 4 × 44k whole mouse genome microarrays (G4122F). Posthybridization image acquisition was performed on an Agilent G2564B scanner. Data were extracted by the Feature Extraction software. Low-intensity spots with a raw signal within 3 SDs from the noise were discarded. Data analysis was performed with Agilent GeneSpring GX Version 7.3 and Microsoft Excel. Each array was normalized by the Lowess algorithm. Differentially expressed mRNAs were identified by the significant analysis of microarray tool. mRNAs with a q value of <0.05 were processed. Their analysis was performed in linear scale.

Real-Time Quantitative PCR. Quantitative (q)PCRs were performed on a Bio-Rad MyIQ thermal cycler (6) using primer sets listed in Table S2. Each sample was run in triplicate to avoid processing-related deviations. Alien RNA was detected as per the manufacturer's instructions (Stratagene).

PC12 Cells and Primary Cultures and Transfection of Basal Forebrain Neurons. PC12 cells were maintained in DMEM containing 10% (vol/vol) FBS, 5% (vol/vol) horse serum, 2 mM L-glutamine, 100 U/mL penicillin, and 100 μg/mL streptomycin (Invitrogen). PC12 cells were serum-starved during NGF-induced differentiation (50 ng/mL; 24 or 48 h).

The medial septal region of embryonic mouse brains was dissected by using a dorsal approach at E16.5 (23). Neurons were enzymatically dissociated and plated at a density of 50,000 cells per well (morphometry) or 200,000 cells per well (biochemistry) in poly-D-lysine (PDL)-coated 24-well plates (6). Primary neuron cultures were maintained in DMEM/F12 (1:1) containing B27 supplement [2% (vol/vol)], L-glutamine (2 mM), penicillin (100 U/mL), and streptomycin (100 μg/mL) (all from Invitrogen) and exposed to drugs applied alone or in combination (Table S3). NGF-mediated TrkA signaling was inhibited by incubating forebrain cultures with AG 879 (50 μM; 6 h at 4 DIV) (24). To efficiently inhibit $p75^{NTR}$ signaling, NGF was premixed with Ro 08-2750 for 1 h on ice (25). Cisplatin (50 μM; 12h) was used to inhibit BRCA1's ubiquitin ligase activity (26, 27).

For siRNA transfection, primary basal forebrain cultures were seeded at a density of 50,000 cells per well (24-well format) in DMEM/F12 (1:1) containing B27 supplement [2% (vol/vol)] and L-glutamine (2 mM). The following day, cultures were cotransfected with a GFP construct (0.5 μg; pmaxGFP; Lonza) used to identify transfectants ("positive control") and either scrambled siRNA (50 pmol; sc-36869; Santa Cruz) or a pool of BRCA1 siRNAs (50 pmol; sc-29824; Santa Cruz) with 1 μL of Lipofectamine 2000 (Invitrogen) for 40 min at 37 °C. Cells were washed once in full growth medium and returned to their original medium for 4 DIV. Cultures were immersion fixed [4% (wt/vol) paraformaldehyde] and processed as above (Fig. 5 *J–J$_2$* and Fig. S6 *E* and *E$_1$*).

We monitored the confluence of primary cultures by using an IncuCyte live-cell imaging system (Essen Instruments) to exclude the contribution of proliferating progenitors (measured from 2 wells/condition; Fig. S3*C*). Morphological parameters, including (*i*) the density of cholinergic neurons (Fig. S3*C*), (*ii*) overall cell numbers, (*iii*) the length and number of neurites, (*iv*) their branching points (including the differential recruitment of CB_1Rs), (*v*) the number and shape of growth cones (e.g., Figs. 2*D*, 3 *B*, *B$_1$*, and *C$_2$*, and 5*I$_1$*), and (*vi*) the subcellular distribution of MGL in individual axons in relation to the growth cone ("delay"; Figs. 3G1 and 5I1), were determined at the time points indicated by analyzing calibrated images in the ZEN2010 imaging software module (Zeiss; $n > 20$ cells per group from at least two independently processed coverslips) (6, 12).

Western Blotting. Cultured neurons and PC12 cells were lysed in modified radioimmunoprecipitation assay (RIPA) buffer (6) containing 5 mM NaF, 5 mM Na_3VO_4, 1% Triton X-100, 0.1% *N*-octyl-β-D-glucopyranoside (Calbiochem), and a mixture of protease inhibitors (Complete, EDTA-free; Roche), denatured in Laemmli's buffer, and analyzed by SDS/PAGE. Membranes were blocked in Odyssey blocking buffer (Li-Cor Biosciences; 1 h), exposed to primary antibodies (Table S1) overnight at 4 °C, developed by appropriate combinations of IRDye800 and IRDye680 antibodies (Li-Cor Biosciences, 1:10,000, 1h), and analyzed on a Li-Cor Odyssey IR imager. β-III-tubulin (TUJ1) served as loading control. Basal forebrains extracted from presymptomatic AD11 and wild-type mice ($n = 4$ per group) were lysed in modified RIPA buffer, resolved by SDS/PAGE using Mini-Protean TGX 4–20% gradient gels (Bio-Rad), and immunoblotted as above. β-Actin served as loading control. Integrated optical densities were determined using the Odyssey software. Experiments were performed in duplicate.

Polyribosome Profiling in PC12 Cells. PC12 cells were lysed [20 million cells per 1,200 μL of lysis buffer (pooled from two 10-cm plates) containing 0.3 M NaCl, 5 mM $MgCl_2$, 15 mM Tris·HCl (pH 8.0), 0.5 mM DTT, cycloheximide (0.1 mg/mL), heparin (1 mg/mL; Sigma), and 1% (vol/vol) Triton X-100] and centrifuged (10 min at 12,000 × *g* and 4 °C) (28). The supernatant was loaded onto a linear sucrose gradient (15–50%) and centrifuged (180 min at 200,000 × *g* and 4 °C). Twelve fractions (900 μL each) were collected, and their RNA content was monitored by spectrophotometry at 254 nm (28) (Fig. 4*D$_1$*). We pooled corresponding fractions from two gradient runs to obtain sufficient mRNA for qPCR analyses. RNA recovery was improved by diluting each sample (1:2) with nuclease-free water before RNA isolation (TriReagent LS; Sigma). Differences in RNA extraction efficacy of the gradient fractions were corrected by spiking equal amounts of Alien qRT-PCR Inhibitor Alert (Stratagene) before RNA isolation. Residual heparin was removed by LiCl precipitation of sucrose-fractionated RNA (2 M, 16h, −20 °C). Trace LiCl was removed by precipitating the samples with Na-acetate (3 M; pH 5.3)/ethanol (−20 °C), washing (75% ethanol), and resuspension in nuclease-free water.

SH-SY5Y Cell Culture, Transfection, and Immunoblotting. SH-SY5Y human neuroblastoma cells were seeded at a density of 400,000

cells per well on PDL-coated six-well plates and cultured in DMEM: Glutamax (Invitrogen) containing 10% (vol/vol) FBS overnight (without antibiotics). Lipofectamine 2000 (5 μL; Invitrogen) was used to transfect SH-SY5Y cells with either nontargeting (scrambled) siRNA (sc-37007) or a pool of BRCA1-specific siRNAs (29) (sc-291219; both at 100 pM per well and from Santa Cruz) overnight. Next, media were replaced, and the cells were serum-starved in DMEM:Glutamax supplemented with 0.1% FBS. SH-SY5Y cells were lysed in modified RIPA buffer three days later (29). MGL immunoblotting was performed as above. TUJ1 was used as loading control.

Statistics. Parametric statistical analyses were performed using Student *t* tests (independent samples design). Statistical significance between bundled and spread growth cones (binary ranking) was analyzed by means of the nonparametric Mann–Whitney *U* test (Fig. 2*D* and Fig. S3*D*). A P level of <0.05 was considered statistically significant. Data were expressed as means ± SEM.

1. Tallini YN, et al. (2006) BAC transgenic mice express enhanced green fluorescent protein in central and peripheral cholinergic neurons. *Physiol Genomics* 27(3):391–397.
2. Ledent C, et al. (1999) Unresponsiveness to cannabinoids and reduced addictive effects of opiates in CB1 receptor knockout mice. *Science* 283(5400):401–404.
3. Zimmer A, Zimmer AM, Hohmann AG, Herkenham M, Bonner TI (1999) Increased mortality, hypoactivity, and hypoalgesia in cannabinoid CB1 receptor knockout mice. *Proc Natl Acad Sci USA* 96(10):5780–5785.
4. Capsoni S, et al. (2000) Alzheimer-like neurodegeneration in aged antinerve growth factor transgenic mice. *Proc Natl Acad Sci USA* 97(12):6826–6831.
5. Ruberti F, et al. (2000) Phenotypic knockout of nerve growth factor in adult transgenic mice reveals severe deficits in basal forebrain cholinergic neurons, cell death in the spleen, and skeletal muscle dystrophy. *J Neurosci* 20(7):2589–2601.
6. Keimpema E, et al. (2010) Differential subcellular recruitment of monoacylglycerol lipase generates spatial specificity of 2-arachidonoyl glycerol signaling during axonal pathfinding. *J Neurosci* 30(42):13992–14007.
7. Berghuis P, et al. (2004) Brain-derived neurotrophic factor controls functional differentiation and microcircuit formation of selectively isolated fast-spiking GABAergic interneurons. *Eur J Neurosci* 20(5):1290–1306.
8. Paria BC, et al. (1998) Effects of cannabinoids on preimplantation mouse embryo development and implantation are mediated by brain-type cannabinoid receptors. *Biol Reprod* 58(6):1490–1495.
9. Hurd YL, et al. (2005) Marijuana impairs growth in mid-gestation fetuses. *Neurotoxicol Teratol* 27(2):221–229.
10. Spano MS, Ellgren M, Wang X, Hurd YL (2007) Prenatal cannabis exposure increases heroin seeking with allostatic changes in limbic enkephalin systems in adulthood. *Biol Psychiatry* 61(4):554–563.
11. Viveros MP, et al. (2012) The endocannabinoid system in critical neurodevelopmental periods: Sex differences and neuropsychiatric implications. *J Psychopharmacol* 26(1): 164–176.
12. Mulder J, et al. (2008) Endocannabinoid signaling controls pyramidal cell specification and long-range axon patterning. *Proc Natl Acad Sci USA* 105(25):8760–8765.
13. Mulder J, et al. (2011) Molecular reorganization of endocannabinoid signalling in Alzheimer's disease. *Brain* 134(Pt 4):1041–1060.
14. Marsicano G, Lutz B (1999) Expression of the cannabinoid receptor CB1 in distinct neuronal subpopulations in the adult mouse forebrain. *Eur J Neurosci* 11(12):4213–4225.
15. Berghuis P, et al. (2007) Hardwiring the brain: Endocannabinoids shape neuronal connectivity. *Science* 316(5828):1212–1216.
16. Ashwell KWS, Paxinos G (2008) *Atlas of the Developing Rat Nervous System* (Academic, San Diego).
17. Paxinos G, Franklin KBJ (2001) *The Mouse Brain in Stereotaxic Coordinates* (Academic, San Diego).
18. Steiner H, Bonner TI, Zimmer AM, Kitai ST, Zimmer A (1999) Altered gene expression in striatal projection neurons in CB1 cannabinoid receptor knockout mice. *Proc Natl Acad Sci USA* 96(10):5786–5790.
19. Sholl DA (1953) Dendritic organization in the neurons of the visual and motor cortices of the cat. *J Anat* 87(4):387–406.
20. Antonucci F, et al. (2012) Cracking down on inhibition: Selective removal of GABAergic interneurons from hippocampal networks. *J Neurosci* 32(6):1989–2001.
21. Giuffrida A, Rodríguez de Fonseca F, Piomelli D (2000) Quantification of bioactive acylethanolamides in rat plasma by electrospray mass spectrometry. *Anal Biochem* 280(1):87–93.
22. D'Onofrio M, et al. (2011) Early inflammation and immune response mRNAs in the brain of AD11 anti-NGF mice. *Neurobiol Aging* 32(6):1007–1022.
23. Schnitzler AC, Lopez-Coviella I, Blusztajn JK (2008) Purification and culture of nerve growth factor receptor (p75)-expressing basal forebrain cholinergic neurons. *Nat Protoc* 3(1):34–40.
24. Rende M, et al. (2006) Role of nerve growth factor and its receptors in non-nervous cancer growth: Efficacy of a tyrosine kinase inhibitor (AG879) and neutralizing antibodies antityrosine kinase receptor A and antinerve growth factor: An in-vitro and in-vivo study. *Anticancer Drugs* 17(8):929–941.
25. Niederhauser O, et al. (2000) NGF ligand alters NGF signaling via p75(NTR) and trkA. *J Neurosci Res* 61(3):263–272.
26. Atipairin A, Canyuk B, Ratanaphan A (2011) The RING heterodimer BRCA1-BARD1 is a ubiquitin ligase inactivated by the platinum-based anticancer drugs. *Breast Cancer Res Treat* 126(1):203–209.
27. Khasabova IA, et al. (2012) Cannabinoid type-1 receptor reduces pain and neurotoxicity produced by chemotherapy. *J Neurosci* 32(20):7091–7101.
28. Johannes G, Carter MS, Eisen MB, Brown PO, Sarnow P (1999) Identification of eukaryotic mRNAs that are translated at reduced cap binding complex eIF4F concentrations using a cDNA microarray. *Proc Natl Acad Sci USA* 96(23):13118–13123.
29. Bromberg KD, Ma'ayan A, Neves SR, Iyengar R (2008) Design logic of a cannabinoid receptor signaling network that triggers neurite outgrowth. *Science* 320(5878): 903–909.

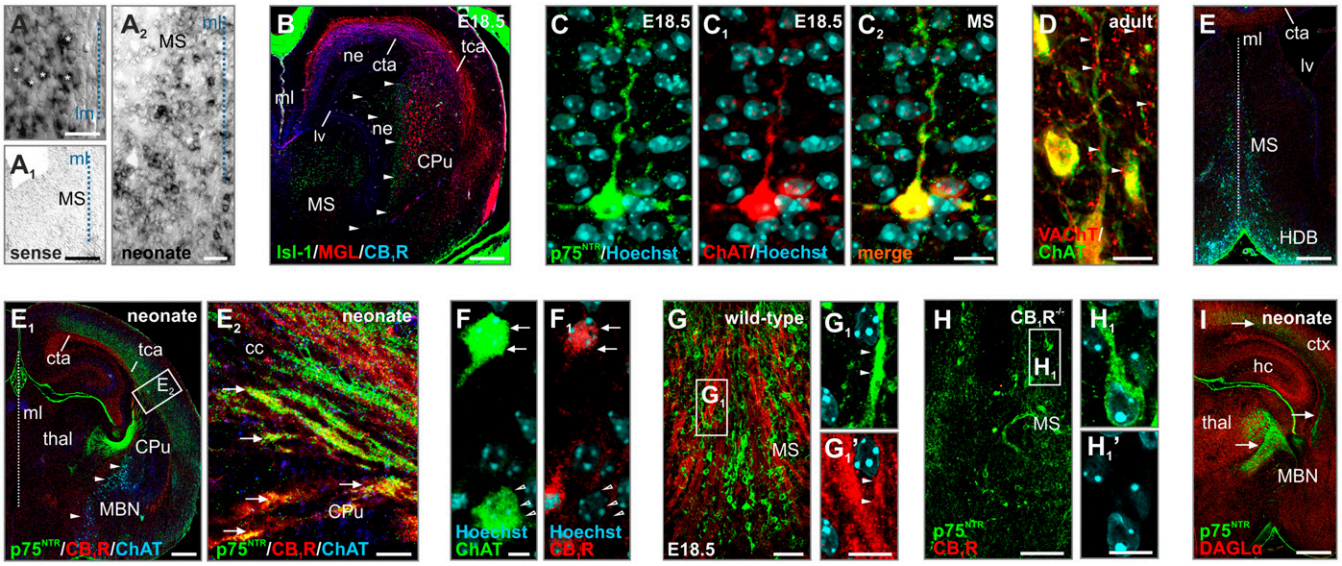

Fig. S1. Distribution of cholinergic neurons and their relation to 2-AG signaling during basal forebrain development. (*A*–*A*$_2$) In situ hybridization signal demonstrating CB_1R mRNA (*) in the MS during late gestation. (*A*$_1$) Sense control showing the lack of nonspecific mRNA hybridization signal. (*B*) Isl-1$^+$ cholinergic progenitors (1) aligned the periventricular neuroepithelium (arrowheads). CPu, caudate putamen/striatum; cta, corticothalamic axon; lv, lateral ventricle; ml, midline; ne, neuroepithelium; tca, thalamocortical axon. (*C*–*C*$_2$) Neonatal cholinergic (ChAT$^+$) neurons were immunoreactive for p75^{NTR}. (*D*) Vesicular acetylcholine transporter (VAChT), shuttling acetylcholine into synaptic vesicles (2), was localized to cholinergic presynapses in the adult. (*E* and *E*$_1$) Distribution of p75^{NTR+} and ChAT$^+$ neurons (arrowheads) in the neonate. thal, thalamus; MBN, magnocellular nucleus basalis. (*E*$_2$) p75^{NTR+} fibers likely harbored CB_1Rs in the corpus callosum (cc) (arrows). (*F* and *F*$_1$) A subpopulation of ChAT$^+$ neurons were immunoreactive for CB_1Rs (arrows) in the fetal basal forebrain. Open arrowheads point to a CB_1R^- cholinergic neuron. (*G*–*G*$_1$′) Colocalization of p75^{NTR} and CB_1Rs in the MS at E18.5 (wild-type fetus). (*H*–*H*$_1$′) We found the complete absence of CB_1R immunoreactivity in the basal forebrain of $CB_1R^{-/-}$ fetuses. Images in *G* and *H* were captured under identical illumination. (*I*) DAGLα distribution by birth resembled the adult expression pattern of this enzyme (3, 4). ctx, cortex. Open rectangles denote the location of the *Insets*. Solid arrowheads define colocalization throughout. (Scale bars: *B*, *E*, *E*$_1$, and *I*, 200 μm; *A*, *A*$_1$, *A*$_2$, *G*, and *H*, 100 μm; *C*$_2$, *D*, and *E*$_2$, 20 μm; *F*, *G*$_1$′, and *H*$_1$′, 10 μm.)

1. Elshatory Y, Gan L (2008) The LIM-homeobox gene Islet-1 is required for the development of restricted forebrain cholinergic neurons. *J Neurosci* 28(13):3291–3297.
2. Roghani A, et al. (1994) Molecular cloning of a putative vesicular transporter for acetylcholine. *Proc Natl Acad Sci USA* 91(22):10620–10624.
3. Tanimura A, et al. (2010) The endocannabinoid 2-arachidonoylglycerol produced by diacylglycerol lipase alpha mediates retrograde suppression of synaptic transmission. *Neuron* 65(3): 320–327.
4. Uchigashima M, et al. (2007) Subcellular arrangement of molecules for 2-arachidonoyl-glycerol-mediated retrograde signaling and its physiological contribution to synaptic modulation in the striatum. *J Neurosci* 27(14):3663–3676.

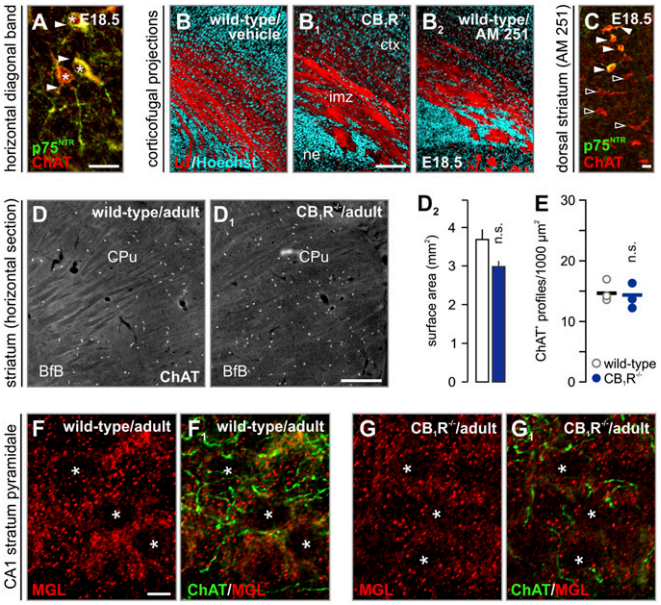

Fig. S2. Genetic and pharmacological manipulation of CB_1Rs misroutes fetal cholinergic projection neurons. (*A*) $p75^{NTR}$ and ChAT colocalized in projection neurons throughout the fetal mouse forebrain, including the HDB. (*B*–*B*$_2$) AM 251 (3 mg/kg), a CB_1R antagonist (8), or vehicle was administered to pregnant wild-type mice with the ensuing axonal phenotype in fetal cortices compared with $CB_1R^{-/-}$ offspring on E18.5. AM 251 introduced axon fasciculation errors reminiscent of the $CB_1R^{-/-}$ phenotype (12). imz, intermediate zone of the fetal neocortex. (*C*) A subset of cholinergic neurons in the rostral dorsolateral striatum unexpectedly coexpressed $p75^{NTR}$ in AM 251-treated fetuses (solid arrowheads). Open arrowheads denote prospective $ChAT^+$ (but $p75^{NTR-}$) striatal interneurons. (*D* and *D*$_1$) Distribution of $ChAT^+$ neurons in the striatum of adult $CB_1R^{-/-}$ and wild-type mice. BfB, basal forebrain. (*D*$_2$) The striatal surface area remained unchanged (n.s., nonsignificant) in $CB_1R^{-/-}$ vs. wild-type mice. (*E*) The density of $ChAT^+$ profiles in the stratum radiatum of the hippocampal CA1 subfield was unchanged upon genetic ablation of CB_1Rs. (*F*–*G*$_1$) The density of MGL^+ puncta was found decreased in the stratum pyramidale of adult $CB_1R^{-/-}$ mice vs. littermate controls. Asterisks label the position of neuronal nuclei. Data were expressed as means ± SEM. (Scale bars: *B*$_1$ and *D*$_1$, 200 μm; *A*, 25 μm; *C* and *F*, 10 μm.)

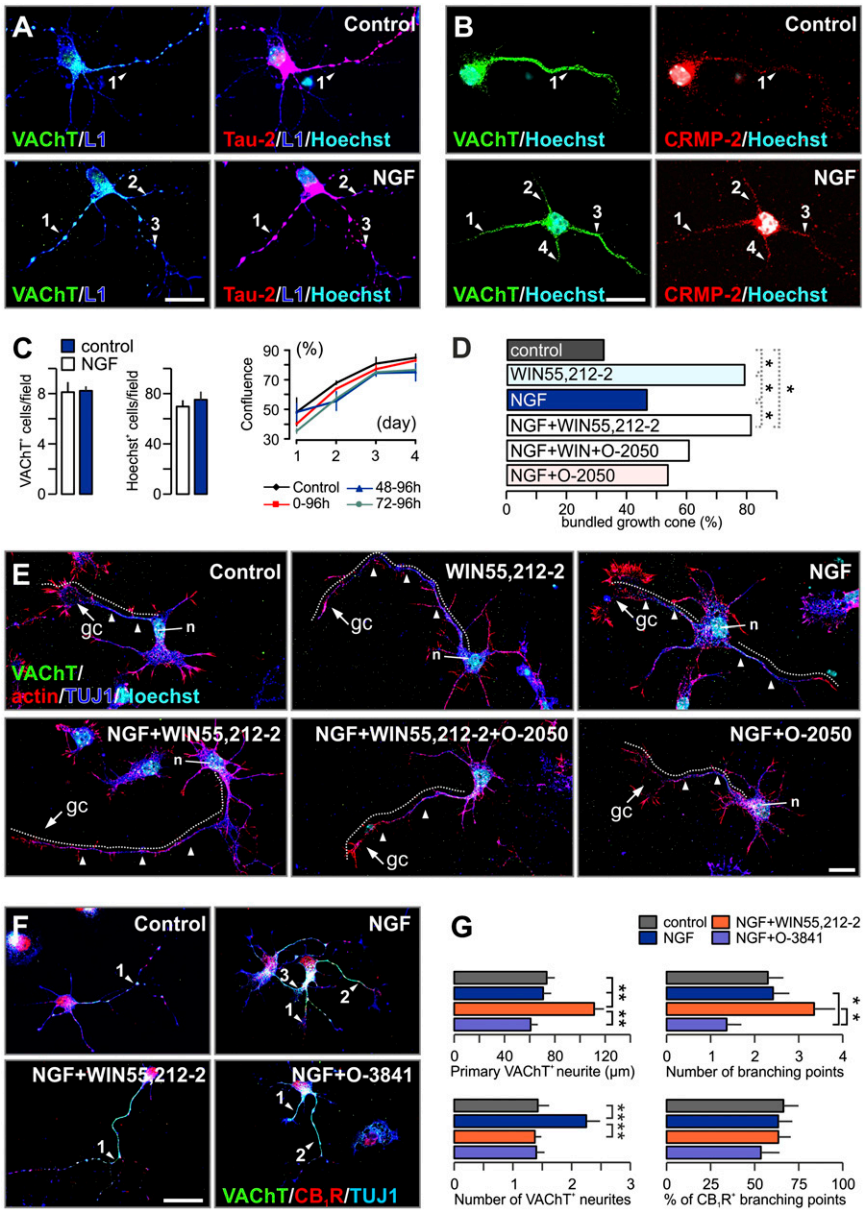

Fig. S3. NGF-induced morphological changes in cultured cholinergic neurons. (*A* and *B*) Cholinergic neurons responded to NGF by forming multiple VAChT$^+$ (*A*) or CRMP-2$^+$ (*B*) neurites, suggesting reduced neuronal polarity. (*C*) NGF did not significantly affect proliferation or survival of cholinergic neurons in basal forebrain cultures. (*D*) WIN 55,212-2 collapsed cholinergic growth cones in a CB_1R-dependent manner, independent of NGF signaling. (*E*) CB_1R antagonism by O-2050 (200 nM) occluded NGF's effects on cholinergic morphology. (*F* and *G*) Likewise, O-3841 prevented the morphological changes induced by NGF. Data were expressed as means ± SEM. $^{**}P < 0.01$, $^{*}P < 0.05$ (Mann–Whitney *U* test in *D* or Student *t* test in *G*). (Scale bar: *A*, *B*, *E*, and *F*, 20 μm.)

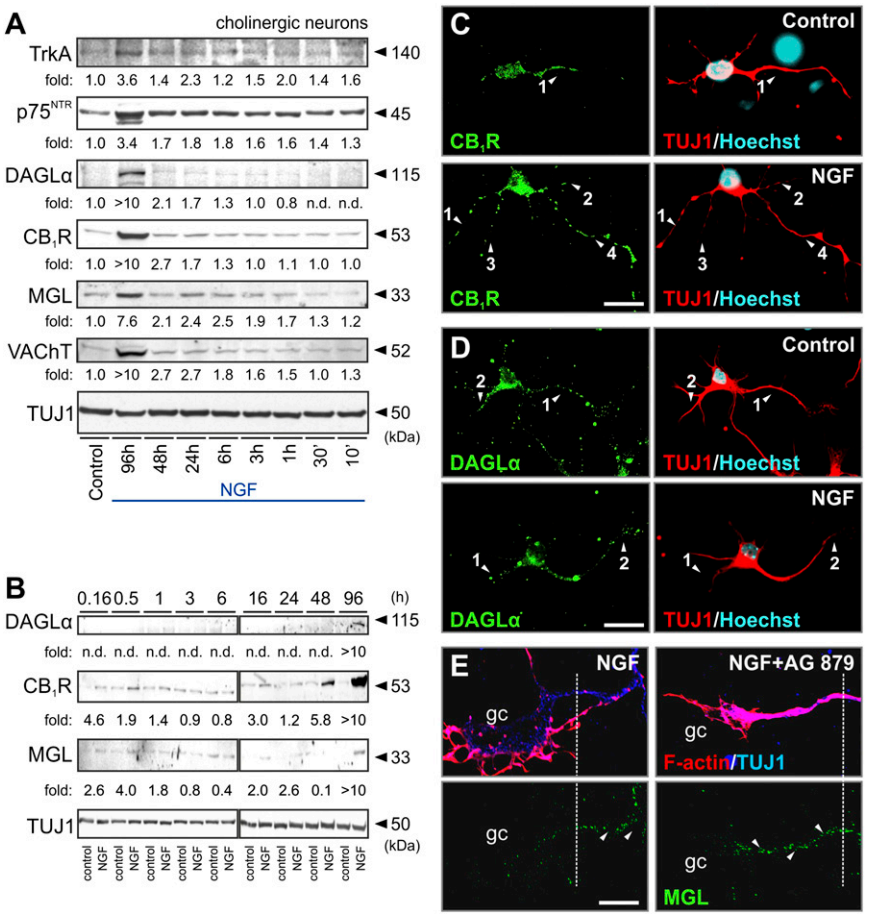

Fig. S4. Time course of NGF-induced up-regulation of 2-AG signaling and the ensuing cholinergic phenotype. (*A* and *B*) Temporal dynamics of the NGF-induced increase in DAGLα, CB_1R, and MGL protein levels in primary cultures from the fetal mouse basal forebrain. Developing neurons expressed both TrkA and $p75^{NTR}$, able to bind NGF in vitro. Note that NGF coincidently induced DAGLα, CB_1R, and MGL expression by 4 DIV in both forward (control at end-point) (*A*) and reverse (*B*) experimental designs. (*C* and *D*) NGF also imposed the subcellular redistribution of CB_1R (*C*) but not DAGLα (*D*) in cholinergic neurons. DAGLα was found trafficked toward both axons and dendrites under physiological conditions in developing neurons (1, 2). (*E*) Inhibition of NGF-mediated TrkA signaling by AG 879 (3) allowed MGL to intrude into the F-actin-rich motile domain of neurites, including the growth cone. (Scale bars: *C* and *D*, 20 μm; *E*, 5 μm.)

1. Mulder J, et al. (2008) Endocannabinoid signaling controls pyramidal cell specification and long-range axon patterning. *Proc Natl Acad Sci USA* 105(25):8760–8765.
2. Bisogno T, et al. (2003) Cloning of the first sn1-DAG lipases points to the spatial and temporal regulation of endocannabinoid signaling in the brain. *J Cell Biol* 163(3):463–468.
3. Rende M, et al. (2006) Role of nerve growth factor and its receptors in non-nervous cancer growth: Efficacy of a tyrosine kinase inhibitor (AG879) and neutralizing antibodies antityrosine kinase receptor A and antinerve growth factor: An in-vitro and in-vivo study. *Anticancer Drugs* 17(8):929–941.

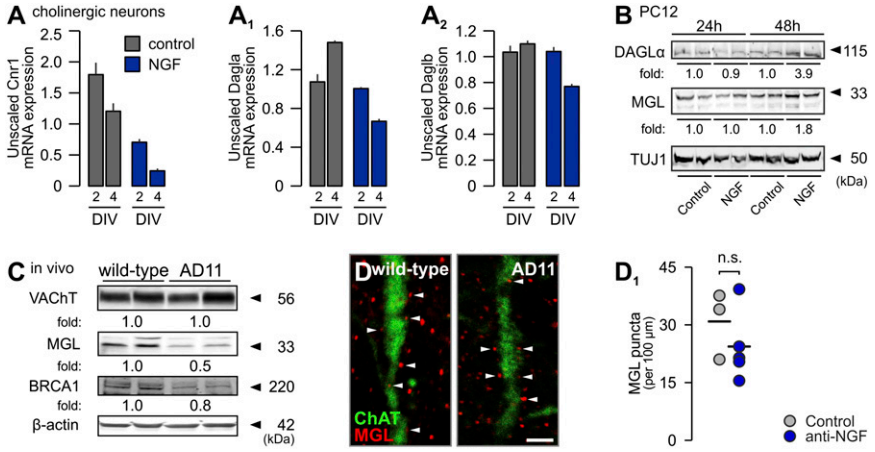

Fig. S5. NGF modulates 2-AG signaling by stabilizing MGL. (*A*–*A*$_2$) CB$_1$R, DAGLα, and DAGLβ mRNA expression in basal forebrain cultures treated with NGF. (*B*) PC12 cells responded to NGF by up-regulating DAGLα and MGL. (*C*–*D*$_1$) We confirmed that NGF regulates MGL protein expression in vivo in mice postnatally expressing a recombinant NGF-neutralizing antibody (AD11 strain) (1–3). We found decreased MGL protein levels by Western blotting (*C*) in conjunction with a marked decline of MGL immunoreactivity along cholinergic dendrites, likely MGL$^+$ presynapses (*D* and *D*$_1$), in basal forebrain territories of AD11 mice. Note that BRCA1 but not VAChT expression was reduced in presymptomatic AD11 mice (*C*). Data were expressed as means ± SEM (n.s., nonsignificant). (Scale bar: *D*$_1$, 3 μm.)

1. Ruberti F, et al. (2000) Phenotypic knockout of nerve growth factor in adult transgenic mice reveals severe deficits in basal forebrain cholinergic neurons, cell death in the spleen, and skeletal muscle dystrophy. *J Neurosci* 20(7):2589–2601.
2. D'Onofrio M, et al. (2011) Early inflammation and immune response mRNAs in the brain of AD11 anti-NGF mice. *Neurobiol Aging* 32(6):1007–1022.
3. Cattaneo A, Capsoni S, Paoletti F (2008) Towards non invasive nerve growth factor therapies for Alzheimer's disease. *J Alzheimers Dis* 15(2):255–283.

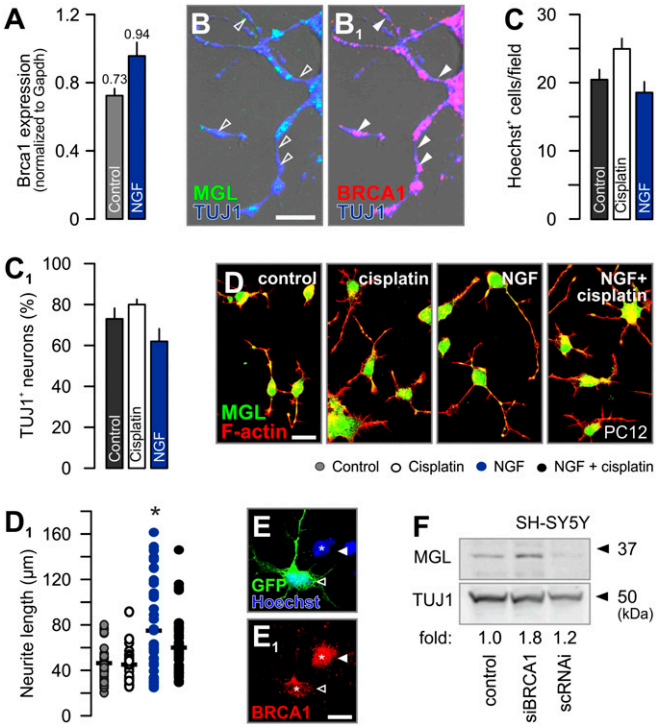

Fig. S6. BRCA1 regulates MGL availability in growth cones. (*A*) In PC12 cells, NGF up-regulated BRCA1 mRNA expression. (*B* and *B*$_1$) Cellular localization of BRCA1 in cultured neurons. Open arrowheads pinpoint the lack of MGL/BRCA1 colocalization in protruding neurites. Cisplatin did not affect cell survival (Hoechst) (*C*) or neuronal differentiation (TUJ1$^+$) (*C*$_1$) in vitro. NGF was used as positive control. (*D* and *D*$_1$) Cisplatin reversed NGF-induced neurite outgrowth in PC12 cells. (*E*) Reduced BRCA1 immunoreactivity (open arrowhead) in basal forebrain neurons confirmed successful knock-down of Brca1 mRNA expression by means of transient transfection with a pool of siRNAs. Cotransfection with a plasmid containing GFP was used to identify transfectants. Nontransfected neighbors retained BRCA1 protein (solid arrowhead). Asterisks point to Hoechst 33,342-stained nuclei. (*F*) siRNA-mediated Brca1 silencing stabilized MGL in SH-SY5Y human neuroblastoma cells in vitro. We chose SH-SY5Y because this cell line coexpresses MGL and BRCA1 at particularly high levels (for reference, see "The Human Protein Atlas"; www.proteinatlas.org). Data were expressed as means ± SEM. *$P < 0.05$ vs. all other groups examined (Student *t* test). (Scale bars: *D*$_1$, 10 μm; *B*, 5 μm.)

Table S1. List of markers used for immunofluorescence labeling

Marker	Host	Histochemistry	Western blotting	Source
β-III-tubulin	Mouse	1:2,000	1:2,000	Promega
β-Actin	Mouse		1:2,000	Sigma
BRCA1	Goat	1:50–1:250		Santa Cruz
BRCA1	Rabbit	1:250	1:250	Abcam
CB_1R (AA400-473)	Guinea pig	1:500	1:500	K.M.
ChAT	Goat	1:100		Millipore
CRMP-2	Mouse	1:500		IBL
DAGLα	Guinea pig	1:500	1:500	K.M.
DAGLβ	Rabbit	1:500	1:500	K.M.
Islet-1	Mouse	1:500		DSHB
L1-NCAM	Rat	1:2,000		Millipore
MAP2	Mouse	1:500		Sigma
MGL (AA171-206)	Rabbit	1:1,000	1:1,000	K.M.
$p75^{NTR}$	Rabbit	1:1,000	1:2,000	Promega
Tau-2	Mouse	1:1,000		Merck
TrkA	Rabbit	1:500		Biosensis
TrkA	Rabbit		1:500	Cell Signaling
VAChT	Rabbit	1:2,000		Synaptic Systems
VAChT	Rabbit		1:1,000	H. Martens

Panel of antibodies applied to study the molecular composition and cell type specificity of 2-AG signaling in developing mouse brain (1). Antibodies have been characterized previously (1–12). Anti-VAChT antibodies used for Western blotting were from H. Martens (Synaptic Systems). DSHB, Developmental Studies Hybridoma Bank; MAP2, microtubule-associated protein-2.

1. Keimpema E, et al. (2010) Differential subcellular recruitment of monoacylglycerol lipase generates spatial specificity of 2-arachidonoyl glycerol signaling during axonal pathfinding. *J Neurosci* 30(42):13992–14007.
2. Mulder J, et al. (2011) Molecular reorganization of endocannabinoid signalling in Alzheimer's disease. *Brain* 134(Pt 4):1041–1060.
3. Berghuis P, et al. (2007) Hardwiring the brain: Endocannabinoids shape neuronal connectivity. *Science* 316(5828):1212–1216.
4. Elshatory Y, Gan L (2008) The LIM-homeobox gene Islet-1 is required for the development of restricted forebrain cholinergic neurons. *J Neurosci* 28(13):3291–3297.
5. Kouznetsova A, et al. (2009) BRCA1-mediated chromatin silencing is limited to oocytes with a small number of asynapsed chromosomes. *J Cell Sci* 122(Pt 14):2446–2452.
6. Li ZS, Furness JB (1998) Immunohistochemical localisation of cholinergic markers in putative intrinsic primary afferent neurons of the guinea-pig small intestine. *Cell Tissue Res* 294(1): 35–43.
7. Nishimura T, et al. (2003) CRMP-2 regulates polarized Numb-mediated endocytosis for axon growth. *Nat Cell Biol* 5(9):819–826.
8. Barbin G, et al. (2004) Axonal cell-adhesion molecule L1 in CNS myelination. *Neuron Glia Biol* 1(1):65–72.
9. Binder LI, Frankfurter A, Rebhun LI (1986) Differential localization of MAP-2 and tau in mammalian neurons in situ. *Ann N Y Acad Sci* 466:145–166.
10. Tremere LA, Pinaud R, Grosche J, Härtig W, Rasmusson DD (2000) Antibody for human p75 LNTR identifies cholinergic basal forebrain of non-primate species. *Neuroreport* 11(10): 2177–2183.
11. Gies U, et al. (2001) Cortical cholinergic decline parallels the progression of Borna virus encephalitis. *Neuroreport* 12(17):3767–3772.
12. Klein R, Jing SQ, Nanduri V, O'Rourke E, Barbacid M (1991) The trk proto-oncogene encodes a receptor for nerve growth factor. *Cell* 65(1):189–197.

Table S2. List of qPCR primers

GenBank accession no.	Primer pair*	T_A (°C)	Position (exon)
NM_007726 (*Cnr1*)			
Forward	5′-TCTTAGACGGCCTTGCAGAT-3′	60	2
Reverse	5′-AGGGACTACCCCTGAAGGAA-3′		2
NM_198114 (*Dagla*)			
Forward	5′-TCATGGAGGGGCTCAATAAG-3′	60	18
Reverse	5′-AGCCCTCCAGACTCATCTCA-3′		20
NM_144915 (*Daglb*)			
Forward	5′-GTGTGCTGTGGTGGATTGTC-3′	60	1/2
Reverse	5′-TCTCATGCTGACACACACGA-3′		2
NM_001166251 (*Mgll*)			
Forward	5′-CAGAGAGGCCAACCTACTTTTC-3′	60	5
Reverse	5′-ATGCGCCCCAAGGTCATATTT-3′		6
NM_008084 (*Gapdh*)			
Forward	5′-AACTTTGGCATTGTGGAAGG-3′	60	4
Reverse	5′-ACACATTGGGGGTAGGAACA-3′		5
NM_009764 (*Brca1*)			
Forward	5′-TGAAGACTGCTCGCAGAGTGATA-3′	60	11
Reverse	5′-AGCTTCCAGGTGAGCCATTTC-3′		12
NM_007193 (*Egr1*)			
Forward	5′-CCACAACAACAGGGAGACCT-3′	60	2
Reverse	5′-ACTGAGTGGCGAAGGCTTTA-3′		2

Quantitative PCR reactions were performed with primer pairs amplifying short fragments for each gene (6). Primer pairs were designed to efficiently anneal to homologous nucleotide sequences from mouse and rat. T_A, annealing temperature. *Egr1*, early growth response protein 1; *Cnr1*, CB_1 cannabinoid receptor.
*Forward and reverse indicate primer orientation.

Table S3. List of ligands used in pharmacological experiments in vitro and in vivo

Ligand	Concentration	Source	Product code	Effect
AG 879	50 μM	Tocris Bioscience	2617	TrkA inhibitor
AM 251	3 mg/kg	Tocris Bioscience	1117	CB1R antagonist
Cisplatin	50 μM	Tocris Bioscience	2251	DNA synthesis/BRCA1 inhibitor
Edelfosine	10 μM	Tocris Bioscience	3022	PLC inhibitor
JZL 184	40 mg/kg	Cayman Chemical	13158	MGL inhibitor
K-252a	100 ng/mL	Calbiochem	480354	Trk inhibitor
Lactacystin	20 μM	Tocris Bioscience	2267	Proteasome inhibitor
LY294002	25 μM	Tocris Bioscience	1130	PI3K inhibitor
NGF-7S	5 or 50 ng/mL	Invitrogen	13290-010	Growth factor
O-2050	200 nM	Tocris Bioscience	1655	CB1R silent antagonist
O-3841	1 μM	V. di Marzo		DAGL inhibitor
PD98059	10 μM	Cell Signaling Technology	9900	MAPK (Erk) inhibitor
PP2	100 nM	Calbiochem	529573	Src inhibitor
Ro 08–2750	1 μM	Tocris Bioscience	1995	p75NTR inhibitor
WIN55,212–2	1 μM	Tocris Bioscience	1038	Cannabinoid receptor agonist

O-3841, a DAGL inhibitor (1), was synthesized by R. Razdan and V. di Marzo (Istituto di Chimica Biomolecolare, Consiglio Nazionale delle Ricerche, I-80078 Naples, Italy). Product codes refer to the suppliers' catalog numbers.

1. Bisogno T, et al. (2006) Development of the first potent and specific inhibitors of endocannabinoid biosynthesis. *Biochim Biophys Acta* 1761(2):205–212.